Supporting Information

Widespread gene editing in the brain via *in utero* delivery of mRNA using acid-degradable lipid nanoparticles

Kewa Gao[1,2,#], Hesong Han[3,#], Matileen G. Cranick[1], Sheng Zhao[3], Shanxiu Xu[1], Boyan Yin[1,3], Hengyue Song[1,5], Yibo Hu[6], Maria T. Clarke[1], David Wang[1,4], Jessica M. Wong[1,4], Zehua Zhao[1], Benjamin W. Burgstone[3], Diana L. Farmer[1,2], Niren Murthy[3,*], Aijun Wang[1,2,4,*]

1. Center for Surgical Bioengineering, Department of Surgery, School of Medicine, University of California, Davis, Sacramento, CA, 95817, United States
2. Institute for Pediatric Regenerative Medicine, Shriners Hospitals for Children, Sacramento, CA, 95817, United States
3. Department of Bioengineering, University of California, Berkeley, Berkeley, CA, 94720, United State.
4. Department of Biomedical Engineering, University of California, Davis, Davis, CA, 95616, United States
5. Department of Burns and Plastic Surgery, The Third Xiangya Hospital of Central South University, Hunan, 410013, China
6. Clinical Research Center, The Second Xiangya Hospital, Central South University, Hunan, 410011, China

* Correspondence to:

Prof. N. Murthy, nmurthy@berkeley.edu

Prof. A. Wang, aawang@ucdavis.edu

[#] These authors contributed equally to the study.

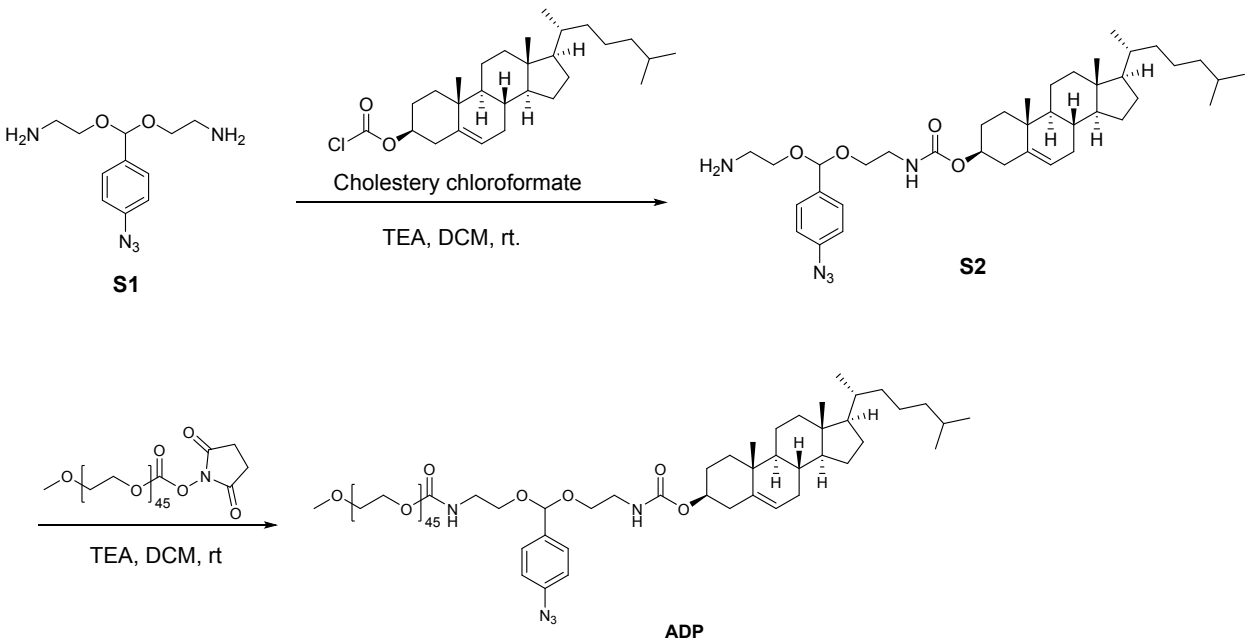

Figure S1. Synthesis of acid degradable PEG-lipid (ADP).

Table S1 Components of ADP-LNP

PEG-lipid	Molar ratios/Molar percentages (%)				
	DOTAP	DLin-MC3-DMA	DOPE	Cholesterol	ADP
10%	35/18.24	45/23.74	22/11.31	70/36.71	19.0/10

Table S2 Components of DLin-MC3-DMA-LNP (Std-LNP)

DLin-MC3-DMA	Molar ratios/Molar percentages (%)			
	PEG2K-DMG	DLin-MC3-DMA	DOPE	Cholesterol
36.8%	2.5/1.18	62/36.8	40/23.82	65/38.2

Table S3 Size and zeta potential characterization of LNPs

LNP	Size (nm)	Zeta potential (mV)
ADP-LNP	86.00 ± 7.98	3.34 ± 1.43
Std-LNP	135.73 ± 28.07	-5.16 ± 2.14

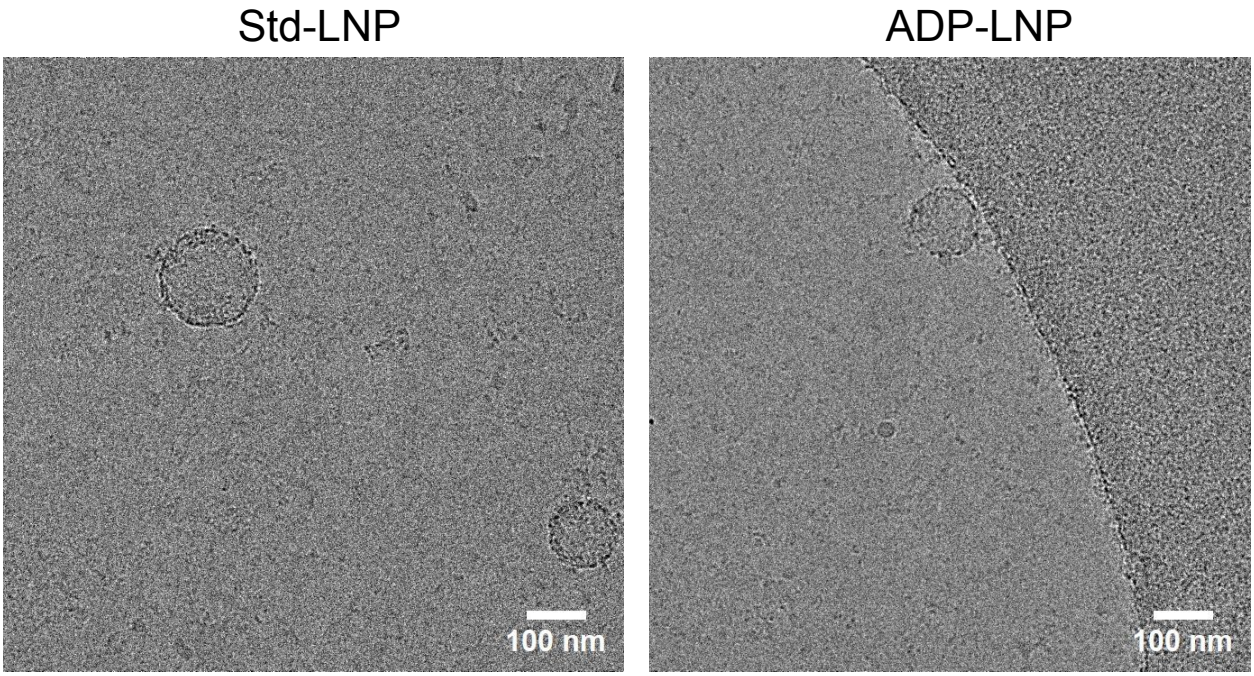

Figure S2. Representative cryo-TEM images for Std-LNP and ADP-LNP.

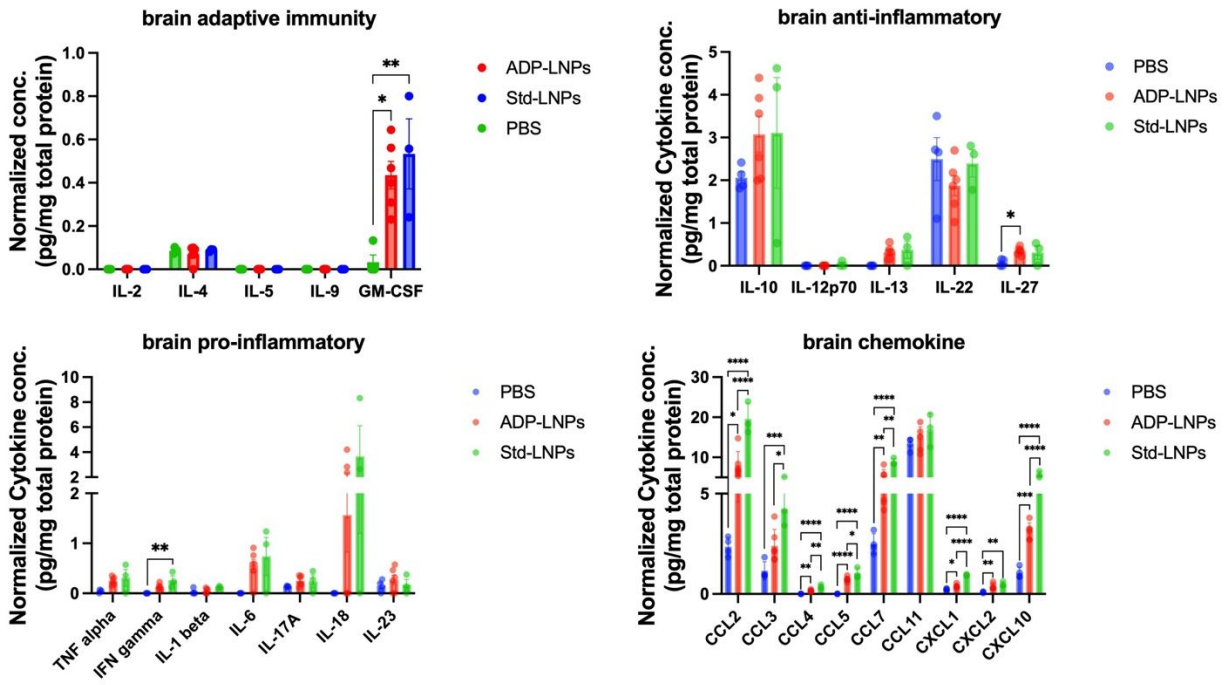

Figure S3 Full panel of cytokine and chemokine expression levels in the mouse brain post fetal injection of LNPs and PBS.

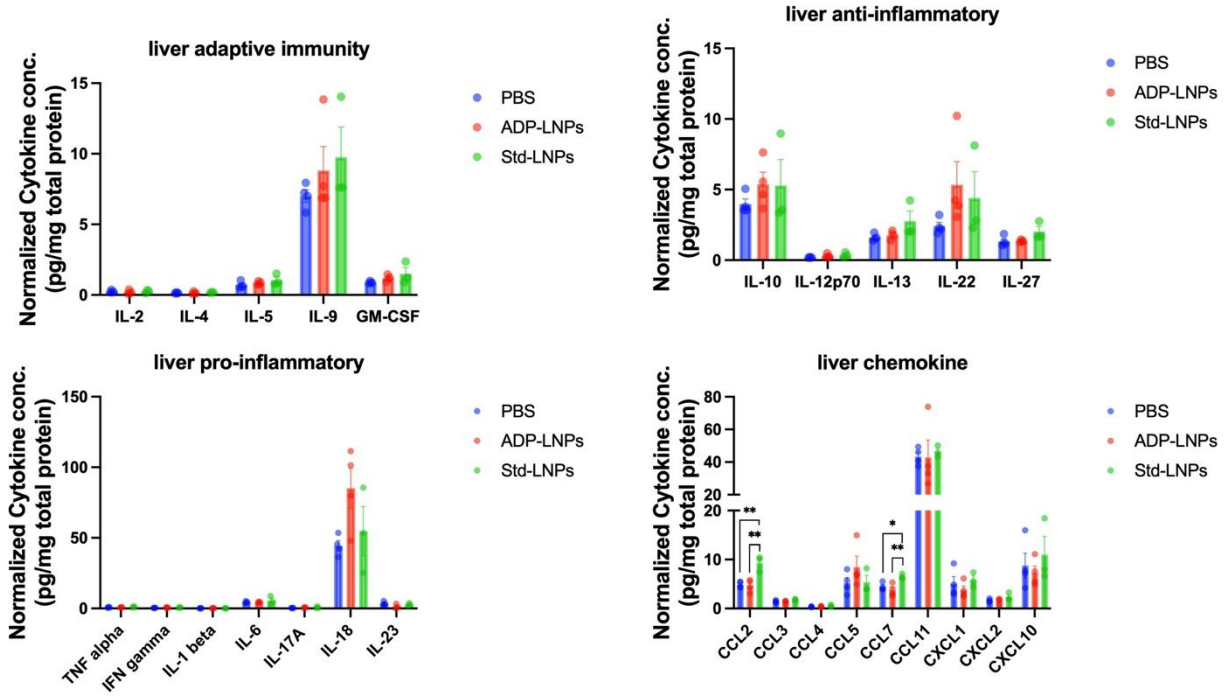

Figure S4. Full panel of cytokine and chemokine expression levels in the mouse liver post fetal injection of LNPs and PBS.

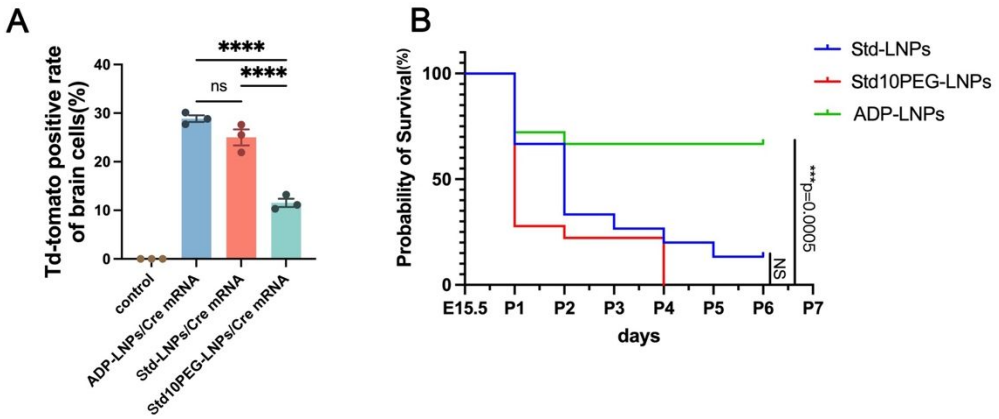

Figure S5. Characterization of the brain transfection efficiency and probability of survival of mice after in utero ICV injection of LNPs

(A) Td-tomato positive rate of brain cells (%) after ICV injection of Cre mRNA encapsulated in ADP-LNPs, std-LNPs, and std10PEG-LNPs was quantified using flow cytometry analyses of all the brain cells dissociated from the entire mouse brain. Data were expressed as mean ± standard deviation: **** $p < 0.0001$ ($n = 3$). (B) Probability of survival (%) following ICV injection of std10PEG-LNPs compared to std-LNPs and ADP-LNPs. Fetuses injected with std-LNPs with both 1% and 10% PEG concentrations exhibited significantly lower survival rates, with no significant difference between the two groups (ns). The survival probability of fetuses injected with ADP-LNPs is significantly higher than the std-LNPs, and std10PEG-LNPs groups (***$p = 0.0005$).

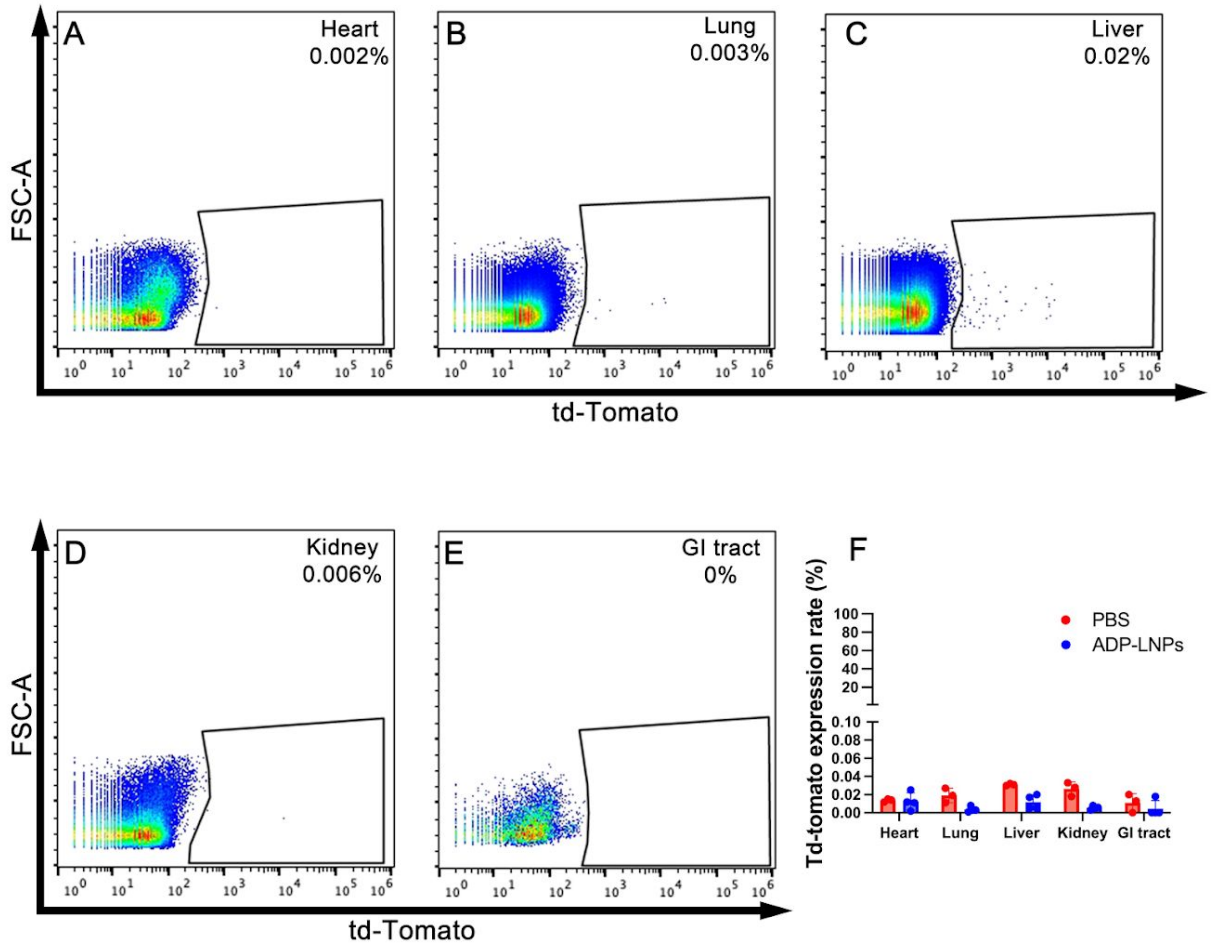

Figure S6. In utero ICV injection of ADP-LNPs did not transfect internal organs outside of the brain

(A-E) Flow cytometry analysis of td-Tomato expression in various organs 48 hours after ICV injection of ADP-LNPs in fetal mice. (F) Summary graph showing td-Tomato expression rates in the heart, lung, liver, kidney, and GI tract, comparing PBS-injected controls (red) and ADP-LNPs-injected fetuses (blue). The data indicates negligible td-Tomato expression in all examined organs, suggesting that ADP-LNPs do not transfect internal organs outside of the brain following in utero ICV injection.

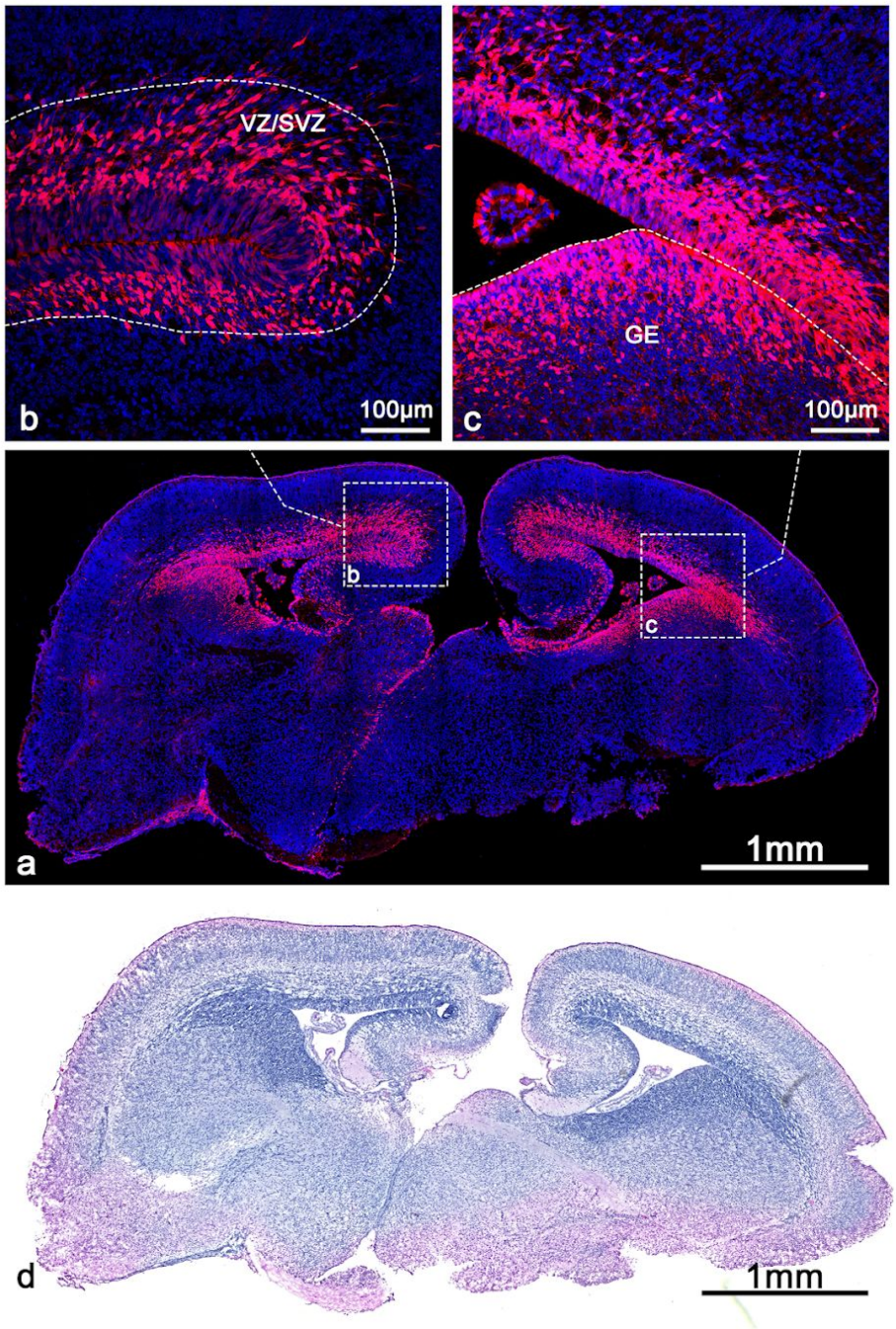

Figure S7. Distribution of transfected cells in the mouse brain after ICV injection of Std-LNPs containing Cre mRNA

(a) Representative whole-brain coronal section showing the overall distribution of td-Tomato positive cells after ICV injection of std-LNPs containing Cre mRNA at E15.5, analyzed 48 hours post-injection. Higher magnification image of the ventricular zone (VZ), subventricular zone (SVZ) (b) and ganglionic eminence (GE) (c) showing extensive transfection in these proliferative regions. (d) HE staining of a similar coronal section showing the overall brain structure for comparison.

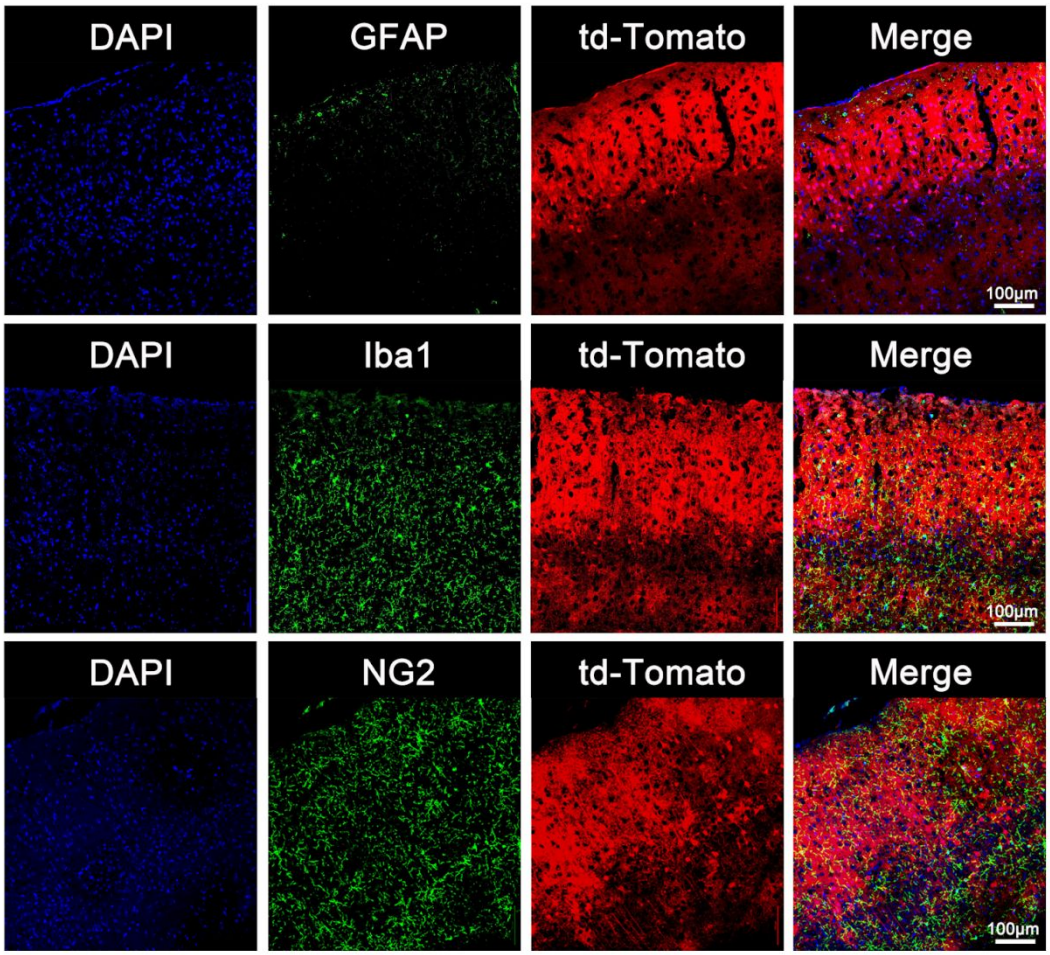

Figure S8. Cellular characterization of ADP-LNP transfection specificity in the mouse cortex

Representative IHC images showed that the majority of transfected cells in the cortex are negative for the astrocyte, microglia and oligodendrocyte markers GFAP, Iba1 and NG2, respectively.

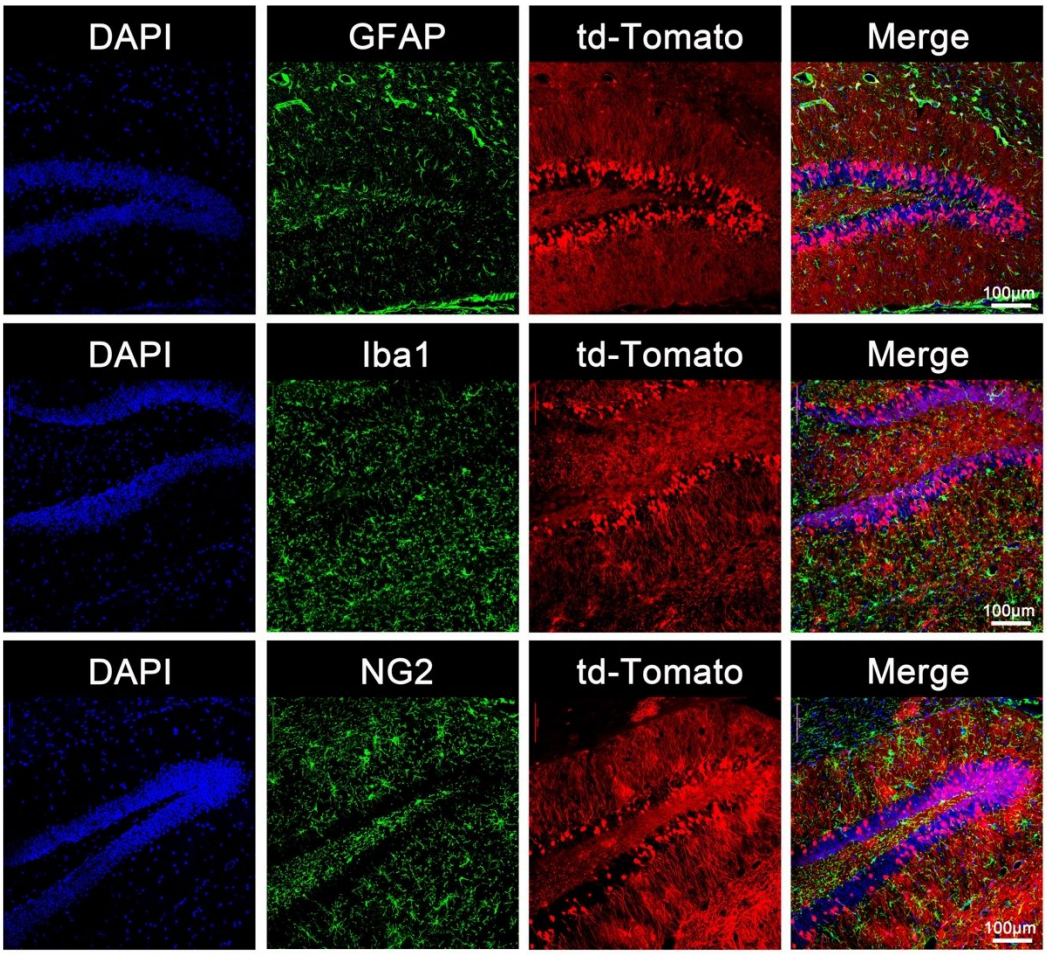

Figure S9. Cellular characterization of ADP-LNP transfection specificity in the mouse hippocampus.

Representative IHC images showed that the majority of transfected cells in the hippocampus are negative for the astrocyte, microglia and oligodendrocyte markers GFAP, Iba1 and NG2, respectively.

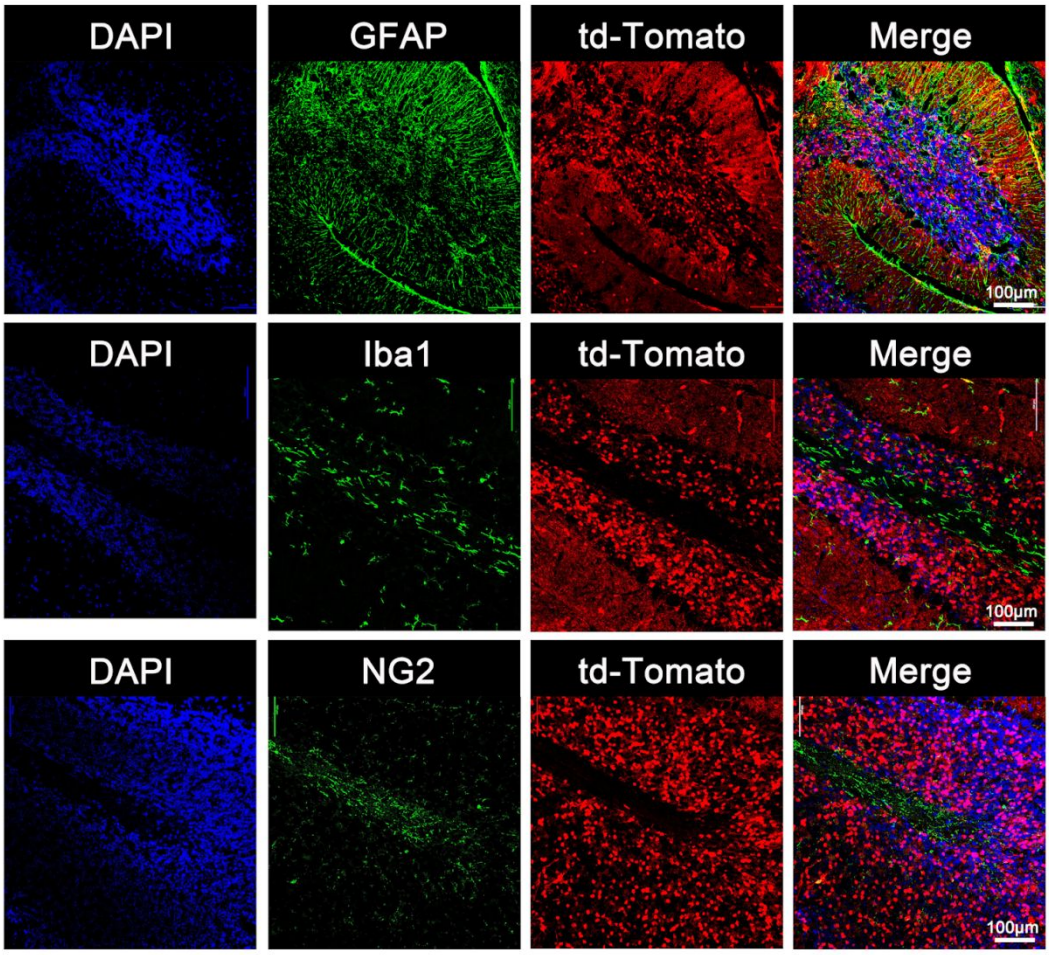

Figure S10. Cellular characterization of ADP-LNP transfection specificity in the mouse cerebellum

Representative IHC images showed that the majority of transfected cells in the cerebellum are negative for the astrocyte, microglia and oligodendrocyte markers GFAP, Iba1 and NG2, respectively.

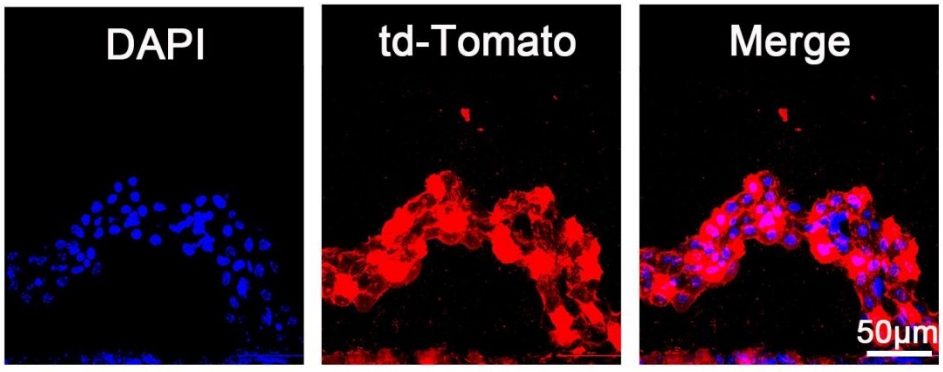

Figure S11. Localization of ADP-LNP/cre mRNA transfected cells in mouse choroid plexus Cells
Representative IHC images showed that the majority of cells in the mouse choroid plexus are transfected following in utero injection of ADP-LNP/Cre mRNA complexes.

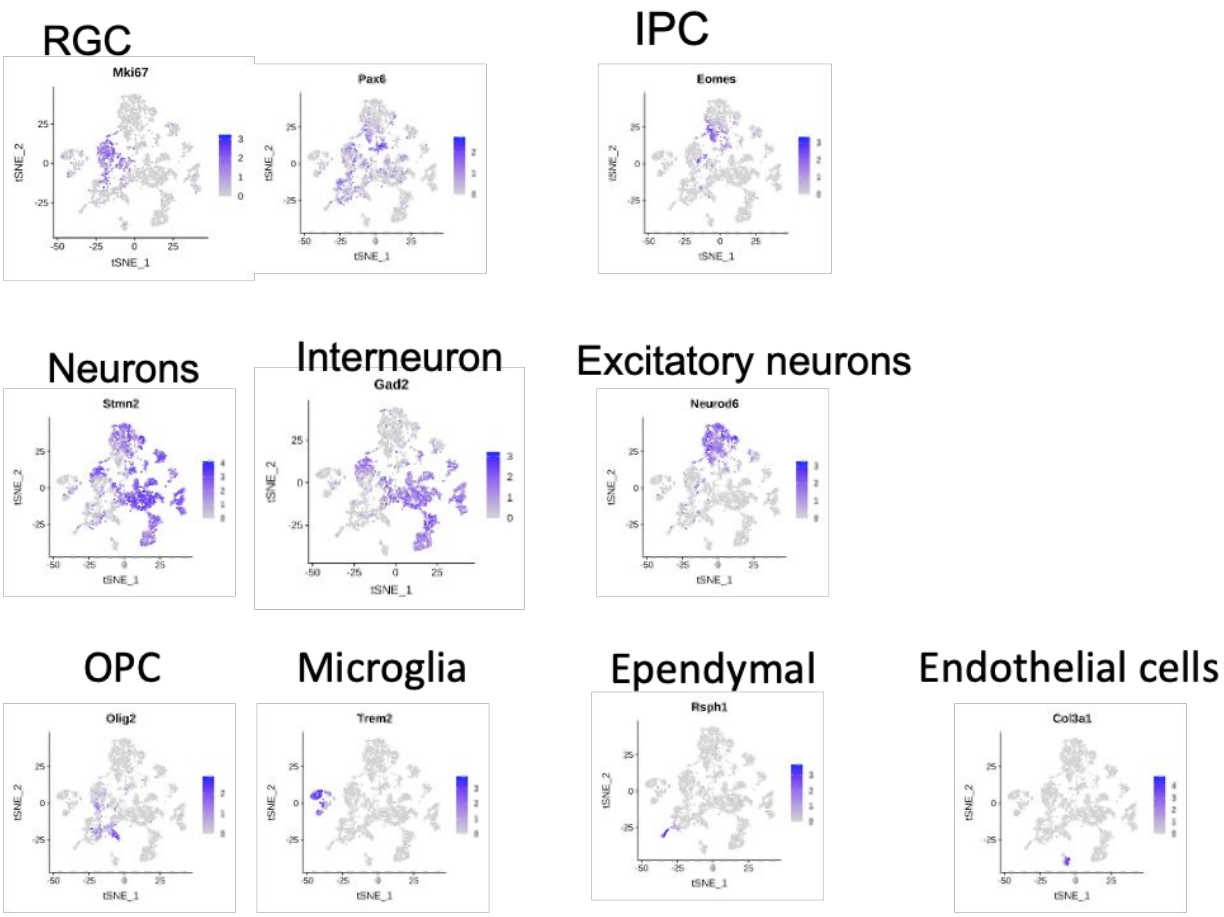

Figure S12. t-SNE analysis of gene expression profiles in transfected brain cells. Expression of cell type specific genes are overlaid with the global tSNE for cell cluster annotation.

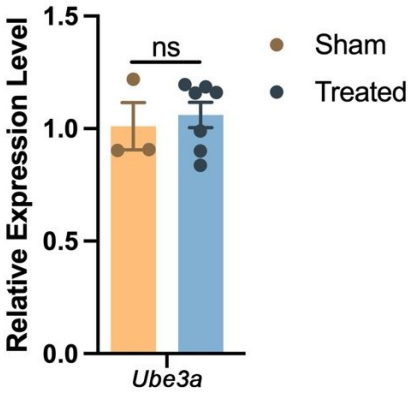

Figure S13. Relative expression levels of *Ube3a* in mice treated with ADP-LNP versus sham groups.